

# Scanning SQUID Imaging of Reduced Superconductivity Due to the Effect of Chiral Molecule Islands Adsorbed on Nb

Meital Ozeri, T.R. Devidas, Hen Alpern,\* Eylon Persky, Anders V. Bjorlig, Nir Sukenik, Shira Yochelis, Angelo Di Bernardo, Beena Kalisky,\* Oded Millo,\* and Yossi Paltiel\*

Unconventional superconductivity was realized in systems comprising a monolayer of magnetic adatoms adsorbed on conventional superconductors, forming Shiba-bands. Another approach to induce unconventional superconductivity and 2D Shiba-bands was recently introduced, namely, by adsorbing chiral molecules (ChMs) on conventional superconductors, which act in a similar way to magnetic impurities as verified by conductance spectroscopy. However, the fundamental effect ChMs have on the strength of superconductivity has not yet been directly observed and mapped. In this work, local magnetic susceptometry is applied on heterostructures comprising islands of ChMs ( $\alpha$ -helix L-polyalanine) monolayers adsorbed on Nb. It is found that the ChMs alter the superconducting landscape, resulting in spatially-modulated weaker superconductivity. Surprisingly, the reduced diamagnetic response is located along the perimeter of the islands with respect to both their interior and the bare Nb. The authors suggest that topological edge-states forming at the edges are the source of the reduced superconductivity, akin to the case of magnetic islands. The results pave new paths for the realization of topological-superconductivity-based devices with changing order parameter.


in many theoretical works.<sup>[3,4]</sup> It was also observed experimentally in transport measurements by the detection of long-range supercurrents in ferromagnetic layers in Josephson  $S$ - $F$ - $S$  junctions<sup>[5-7]</sup> and scanning tunneling spectroscopy (STS) on the superconductor side of  $S$ - $F$  junctions,<sup>[8-10]</sup> confirming theoretical predictions.<sup>[4,11]</sup> The interest in  $S$ - $F$  hybrid systems has vastly expanded over the past decade with the understanding that such systems can open new routes to the realization of topological superconductivity. The observations<sup>[12-15]</sup> of zero-energy Majorana bound states at the ends of magnetic adatoms chains placed on singlet  $s$ -wave superconductors has provided strong support for the concept of creating topological superconductivity in engineered  $S$ - $F$  systems. Concomitantly, it was also proposed that 2D topological superconductivity can be created by placing islands of magnetic adatoms on  $s$ -wave superconductors.<sup>[16-20]</sup>

## 1. Introduction

Spin-triplet superconductivity raised great interest for “superconducting spintronics”,<sup>[1,2]</sup> where equal-spin triplet pairs can be used to carry spin information with low energy dissipation (while in conventional spin-singlet superconductors the Cooper pair has zero net spin polarization). This field was based so far mainly on hybrid systems comprising superconductors ( $S$ ) and ferromagnets ( $F$ ). Such unconventional superconductivity was studied

Compelling experimental evidence for these predictions was gained in the past few years, where topological superconductivity and zero-energy Majorana edge-states were observed in magnetic monolayer islands grown on conventional superconductors. STS measurements showed a significant enhancement of the density of states inside the superconducting gap,<sup>[21]</sup> or the emergence of zero-bias conductance peaks<sup>[22]</sup> on the edges of the ferromagnetic islands deposited on a superconductor. In these studies, the spectra measured on the edges of the islands

M. Ozeri, H. Alpern, N. Sukenik, S. Yochelis, Y. Paltiel  
 Applied Physics Department and the Center  
 for Nanoscience and Nanotechnology  
 The Hebrew University of Jerusalem  
 Jerusalem 91905, Israel  
 E-mail: hen.alpern@mail.huji.ac.il; paltiel@mail.huji.ac.il

 The ORCID identification number(s) for the author(s) of this article can be found under <https://doi.org/10.1002/admi.202201899>.

© 2023 The Authors. Advanced Materials Interfaces published by Wiley-VCH GmbH. This is an open access article under the terms of the Creative Commons Attribution License, which permits use, distribution and reproduction in any medium, provided the original work is properly cited.

DOI: 10.1002/admi.202201899

M. Ozeri, H. Alpern, O. Millo  
 Racah Institute of Physics  
 and the Center for Nanoscience and Nanotechnology  
 The Hebrew University of Jerusalem  
 Jerusalem 91905, Israel  
 E-mail: milode@mail.huji.ac.il

T.R. Devidas, E. Persky, A. V. Bjorlig, B. Kalisky  
 Department of Physics and Institute  
 of Nanotechnology, and Advanced Materials  
 Bar-Ilan University  
 Ramat Gan 5290002, Israel  
 E-mail: beena@biu.ac.il

A. Di Bernardo  
 Physics Department  
 University Konstanz  
 78464, Konstanz Germany

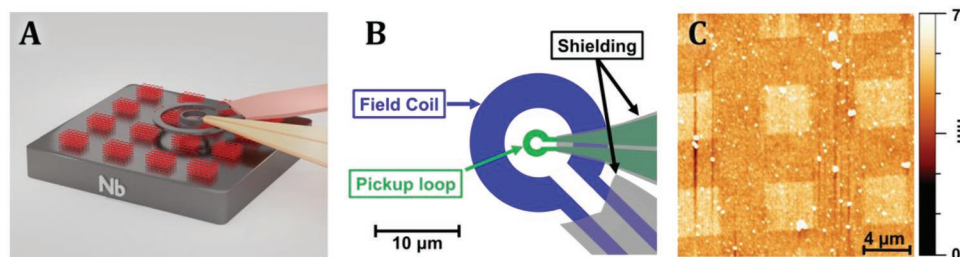


**Figure 1.** A) Schematics of the measurements configuration: a SQUID scanning over sample comprising islands of ChMs adsorbed on a superconducting Nb thin film. B) Details of the scanning SQUID device: a pick-up loop at the centre of a field coil. Alternating current in the field coil applies an alternating magnetic field to the sample and the Meissner response of the film is then detected by the SQUID pick-up loop (more information is provided in the Experimental Section). (C) AFM topographic image showing  $4 \times 4 \mu\text{m}^2$  square-shaped areas of adsorbed ChMs (L-AHPA) on an Nb film.

were distinctly different from those measured in their interior and on the bare superconductor.

Spin-triplet superconductivity and magnetic-like states were shown to be induced in a conventional superconductor via the adsorption of chiral molecules (ChMs) that are non-magnetic in solution. This was demonstrated using a variety of techniques, including STS,<sup>[23,24]</sup> transport measurements on devices,<sup>[25,26]</sup> and muon spin rotation/relaxation.<sup>[27]</sup> The signature of chiral-induced equal-spin superconductivity was found for various superconductors – Nb, proximitized Au/Nb bilayers, and NbSe<sub>2</sub>. The ability of such non-magnetic molecules to generate magnetic-like effects was observed also in other cases, as they have shown the ability to magnetize a ferromagnet<sup>[28]</sup> and enhance magnetism in gold.<sup>[29]</sup> This rich variety of phenomena was attributed to the chiral-induced spin selectivity (CISS) effect observed in ChMs, in which electron transport through chiral electrostatic potentials was shown to be spin-selective.<sup>[30]</sup> A clear demonstration of ChMs acting as magnetic impurities upon adsorption is that when they are sparsely adsorbed on a superconductor (NbSe<sub>2</sub>) they introduce in-gap Yu-Shiba-Rusinov states (Shiba states), akin to the effect of magnetic impurities.<sup>[25]</sup> With increasing density, “Shiba-bands” are constructed from an array of coupled magnetic impurities on a superconducting surface. Even in the case of disorder, as may be the case of adsorbed ChMs, above a critical density the Shiba states hybridize to form a Shiba-glass system, for which a finite net out-of-plane magnetization could induce topological superconductivity, supporting chiral edge modes.<sup>[16,17,31]</sup> As described in Ref. [25], when the ChMs were more densely adsorbed on NbSe<sub>2</sub>, STS shows evidence for a collective phenomenon of hybridized Shiba-like states manifested by the appearance of a zero bias conductance peak that diminishes, but does not split, with increasing magnetic field. This observation is consistent with the above prediction of Shiba-bands forming with increasing density of magnetic impurities.

It is important to note that the above studies show that ChMs act in similar way to magnetic impurities, and consequently it is possible that the ChMs/Superconductor system can also support edge modes. However, there is no direct mapping of the superconducting state that is induced by the ChMs on the surface of superconductors. In standard superconductors the density of states is high, thus the effect of the ChMs on the superconducting state could be hard to distinguish. Therefore, we employed local susceptibility measurements to map and compare the superconducting state in areas where molecules

are adsorbed as compared to bare areas. While there has not yet been any direct indication for edge-states in hybrid ChMs/conventional-superconductor systems, such topological edge-states can cause modulations in the superfluid density that can be detected via local magnetic measurements.<sup>[32]</sup>

Here, we use a scanning superconducting quantum interference device (SQUID) microscope as a local susceptometer<sup>[33–38]</sup> to study ChMs islands adsorbed on the surface of Nb or Au/Nb bilayer films (see Experimental Section for details). Local susceptometry provides access to the spatial distribution of the superfluid density, allowing a direct investigation of the effect of ChMs islands on the superconductivity. On Nb films, we observe reduced diamagnetism on the edges of all ChMs islands with respect to the bare Nb regions and the interior of the islands. In contrast, for the Au/Nb bilayer system, reduced diamagnetic response was found all over each island with no edge modulations.

## 2. Results and Discussion

Susceptibility and magnetometry measurements were carried out using a scanning SQUID microscope. **Figure 1A** depicts the measurement geometry and **Figure 1B** details the various components of the SQUID. Alternating current in the field coil provides the magnetic field to which the Meissner response of the film is measured using a SQUID pick-up loop. The magnetic susceptibility of the sample is proportional to the magnetic flux through the pick-up loop per unit current in the field coil ( $A$ ), and thus measured in units of  $\Phi_0/A$ , where  $\Phi_0 = h/2e$  is the superconducting magnetic flux quantum,  $h$  is the Planck constant, and  $e$  is the electron charge.

The samples were prepared using standard e-beam lithography and lift-off techniques to define the areas of ChMs adsorption on the Nb or Au/Nb bilayer films (see Experimental Section for details). The chiral molecules used in this study are  $\alpha$ -helix L-polyalanine (L-AHPA), and for control experiments we used non-chiral 12-mercaptododecanoic acid (MDA) molecules. L-AHPA ChMs have been shown to arrange as an ordered monolayer on substrates onto which they are adsorbed.<sup>[39]</sup> Transport measurements performed on a non-patterned ChMs/Nb sample show  $\approx 18\%$  reduction in the critical current of the Nb following ChMs-adsorption, but no measurable change in the critical temperature ( $\approx 8.3$  K, see Figure S1, Supporting Information). The decrease in the critical current

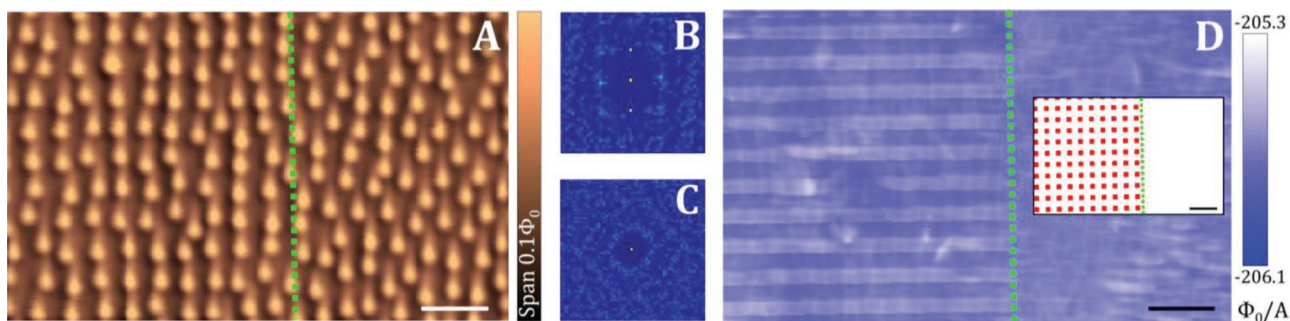


**Figure 2.** A) Magnetometry image of  $2 \times 2 \mu\text{m}^2$  squares of ChMs adsorbed on a 60 nm thick Nb film, taken at 4.2 K after field-cooling at 0.85 G. The dashed green lines in panels A and D mark the boundary between the regions with (left) and without (right) the array of ChMs-islands. A square-like vortex lattice is identified in the adsorption region and absent in the bare region. This is reflected in the 2D FFT images of B) the adsorbed and C) bare regions, derived from the image in panel A. D) Susceptometry measurement taken simultaneously with the magnetometry scan presented in panel A, exhibiting ordered modulation only in the adsorption region, associated with reduced magnetization (see text), assisting the identification of the boundary between the two regions. Inset: Schematic of the designed ChMs islands array. Scale bars  $\sim 10 \mu\text{m}$ .

may be attributed to a smoothing of the pinning potential, as previously observed.<sup>[40]</sup> An atomic force microscopy (AFM) topographic image of a Nb film with adsorbed square-shaped islands of L-AHPA ChMs is shown in Figure 1C, exhibiting a uniform adsorption on all areas. The height of the adsorbed areas is  $2.3 \pm 0.5 \text{ nm}$ , as determined from the AFM measurement (Figure 1C), whereas the length of the L-AHPA molecules is calculated to be  $5.4 \text{ nm}$ ,<sup>[41]</sup> implying a single monolayer of molecules that are tilted with respect to the normal to the surface by  $\approx 65^\circ$ , a tilt angle that is consistent with a previous study.<sup>[42]</sup> The quality of L-AHPA adsorption on Nb was also confirmed using scanning Kelvin probe force microscopy, X-ray photoelectron spectroscopy, and contact angle measurements (Figures S2–S4, Supporting Information).

Mapping the vortex configuration on a ChMs/Nb sample (60 nm thick Nb) can reveal information on the influence of the adsorbed ChMs on vortex dynamics. The vortex configuration was recorded after cooling the sample while applying a constant magnetic field (Figure 2A). The scanned area consists of  $2 \times 2 \mu\text{m}^2$  ChMs-islands arranged in a periodic square lattice pattern (to the left of the vertical green dotted line in Figure 2), and a bare Nb region (to the right), shown schematically in Figure 2B (inset). The boundary between the two regions can be clearly identified by a simultaneous susceptometry scan that shows ordered susceptibility modulations corresponding to the adsorption geometry (Figure 2D). The modulation is associated with reduced diamagnetism of the Nb around the adsorbed ChMs islands, as shown in Figure 3 and further discussed below. The vortex configuration in the region with the ChMs-islands is strikingly different than that of the bare Nb region. Importantly, the vortices in the adsorption region form a nearly periodic square lattice, which is rather unique. This is demonstrated by the 2D FFT (Fast Fourier Transform) images derived from the two regions, presented in Figure 2B,C. A clear cubic symmetry is apparent only for the case of the ChMs-adsorbed region. Such a vortex array structure signifies a pronounced alteration of the pinning-sites configuration following the adsorption geometry,<sup>[43]</sup> highlighting the effect the adsorbed ChMs have on the superconducting properties of the Nb substrate. The vortex density is  $\approx 5 \times 10^{10} \text{ m}^{-2}$ , in accordance with the magnetic field that was applied during the scan

(0.85 G, resulting in a calculated vortex density of  $\approx 4 \times 10^{10} \text{ m}^{-2}$ ). The distance between vortices is  $\approx 2 \mu\text{m}$ , matching the spacing between and the size of the ChMs-islands. This indicates that the islands constitute strong pinning sites, probably due to reduced superconductivity, as observed on their edges in the susceptibility measurements presented below.

Susceptibility mapping measurements performed on a different region of the same ChMs/Nb sample show reduced diamagnetism at the edges of the adsorbed islands (Figure 3A) with respect to the bare Nb regions and interior of the islands. The islands of adsorbed molecules in this study varied in width between 2 to  $30 \mu\text{m}$ , and the edge modulations were seen in islands in this size range, with no detectable size-dependence. An additional measurement on a different ChMs/Nb sample showing the same effect is presented in Figure S5A (Supporting Information). It should be noted here that the contrast which we observe at the edges could also be explained by weak local paramagnetism at the edges that is unrelated to the superconductivity. However, in such a scenario, the paramagnetic signal should also be observed above the superconducting critical temperature ( $T_C \approx 8.3 \text{ K}$ ), when superconductivity-related signals are absent. The lack of such signal above  $T_C$ , as demonstrated by Figure 3B, indicates that the edge effect is exclusively related to the superconducting properties of the hybrid ChMs/Nb region. However, it is possible that a paramagnetic signal related to an emergent unconventional superconductivity contributes to the edge effect, possibly along with the reduced diamagnetism, as we discuss below. Moreover, since the adsorption of ChMs on Nb within each island is uniform (as shown in Figure 1C), we can suggest that the edge signal is of a topological origin, most likely relating to the unconventional superconductivity that emerges in the ChMs-adsorbed areas as shown in our previous studies.<sup>[23–27]</sup> The fact that the reduced diamagnetism (and possibly paramagnetic contribution) appears mainly on the edges of the adsorbed areas is in accordance with previous studies<sup>[21,22]</sup> of monolayer ferromagnetic islands on superconductors, where gap-structure modulations (and in particular the appearance of a zero-bias conductance peak) were more pronounced on the perimeter of the islands. Importantly, the results presented in Figure 3A and Figure S5A (Supporting Information) imply that the

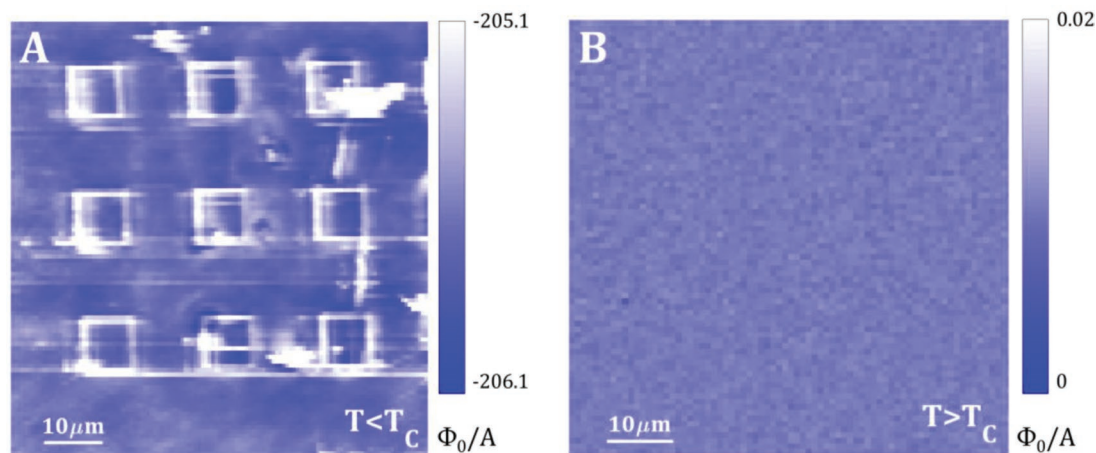


**Figure 3.** Susceptometry images of an Nb film (60 nm thick) with patterned  $8 \times 8 \mu\text{m}^2$  squares of L-AHPA ChMs adsorption, taken A) below  $T_C$ , at 4.2 K, and B) above  $T_C$ , at 19.5 K. Some line- and puddle-shaped regions with a weaker diamagnetic reading can be found off the patterns. These are related to dragging of non-magnetic particles by the SQUID sensor, yet not hindering the genuine magnetic signal on the edges.

ChMs form a monolayer of magnetic impurities, constituting a system similar to the magnetic monolayers studied theoretically<sup>[16,17,31]</sup> and experimentally,<sup>[21,22]</sup> showing the appearance of edge-modes. It should be noted that the SQUID images, such as Figure 3A, are not free of noise and there are locations aside the edges showing signals which are not related to the squares, but these are sporadically dispersed and could be associated with local sample imperfections.

The relatively large width of the edge modulations ( $\approx 1 \mu\text{m}$ ), compared to edge-states measured via STS that appear to be confined to a few nanometers from the edge,<sup>[21,22]</sup> is due to a combination of the experimental resolution (diameter of the SQUID pick-up loop being  $1.5 \mu\text{m}$  in the present measurement) and the scale of the measured phenomena (far-field magnetic response in our experiment as opposed to atomic-scale states measured with a higher resolution STM tip).

A reference sample with adsorbed non-chiral MDA molecules adsorbed on it shows weak modulations in susceptibility (Figure S5B, Supporting Information). This is not surprising, as similar effects of monolayer non-chiral molecules adsorption on the properties of superconductor films has been demonstrated.<sup>[44,45]</sup> However, no distinct edge modulations are seen. This is in vast contrast to the samples with ChMs adsorption in which a strong contrast is clearly seen at all edges.

Motivated by our previous STS study that revealed chiral-induced unconventional superconductivity also on systems of ChMs adsorbed on Au/Nb bilayer films,<sup>[24]</sup> where superconductivity is proximity-induced in the Au film, we performed scanning SQUID susceptometry measurements also for such a hybrid system. To that end, L-AHPA ChMs and non-chiral MDA molecules were adsorbed in a patterned manner onto a 3 nm thick gold film deposited on top of a 60 nm thick Nb film. A typical SQUID scan for the ChMs/Au/Nb system, presented in Figure 4A, shows a nearly uniform reduction of diamagnetism all over the adsorbed islands with respect to the bare Au/Nb regions, with no observable edge modulations. We also present in Figure 4B a measurement performed on a control MDA(non-chiral)/Au/Nb sample, also exhibiting intra-island

reduced diamagnetism, although to a lesser extent. Additional measurements of the two samples showing similar results are depicted in Figure S6 (Supporting Information).

To explain the observations on the Au/Nb bilayers, we note that both the chiral L-AHPA and non-chiral MDA molecules adsorb to the Au surface via a thiol-Au bond, which is known to induce weak magnetism in the gold.<sup>[46–49]</sup> This effect can account for the reduced diamagnetism seen on the entire adsorption areas for both the chiral and non-chiral cases, although the effect is significantly stronger for the L-AHPA molecules due to the chirality of the molecules.<sup>[29,50,51]</sup>

A question still remains as to the lack of reduced diamagnetism at the edges of the ChMs/Au/Nb islands, in particular when triplet-pairing superconductivity was found<sup>[24]</sup> in this system. To explain this, we note that while edge-states are predicted to exist in a system comprising a magnetic monolayer on top of a superconductor, no such edge-states are guaranteed to exist for the case of a 3D magnetic layer on a superconductor. In the ChMs/Nb systems, the ChMs layer behaves as a monolayer of magnetic impurities, as suggested in a previous study,<sup>[25]</sup> and the signature of edge-states is indeed seen in the susceptometry scans. However, in the case of Au/Nb bilayers, the magnetized Au behaves as a 3D “bulk” magnetic layer above the superconductor. Such a system is no longer described by the theory of a 2D Shiba-glass system and does not necessarily support edge-states.

This outcome is demonstrated also by a similar susceptibility contrast seen on ferromagnetic Ni islands (thickness, 7 nm) deposited on an Nb film (Figure 4D,E) that shows no measurable edge modulations. We note that magnetometry measurements can clearly detect and map the magnetization signal from the Ni islands (Figure 4C), but not from the ChMs islands adsorbed on Au/Nb. This implies that even the weak magnetism induced in Au is enough to hinder the formation of edge-states.

Our results provide the first susceptibility mapping of the unique effect that ChMs have on a conventional superconductor upon adsorption. They also extend the realm of adsorption-related emergent phenomena observed by conductance

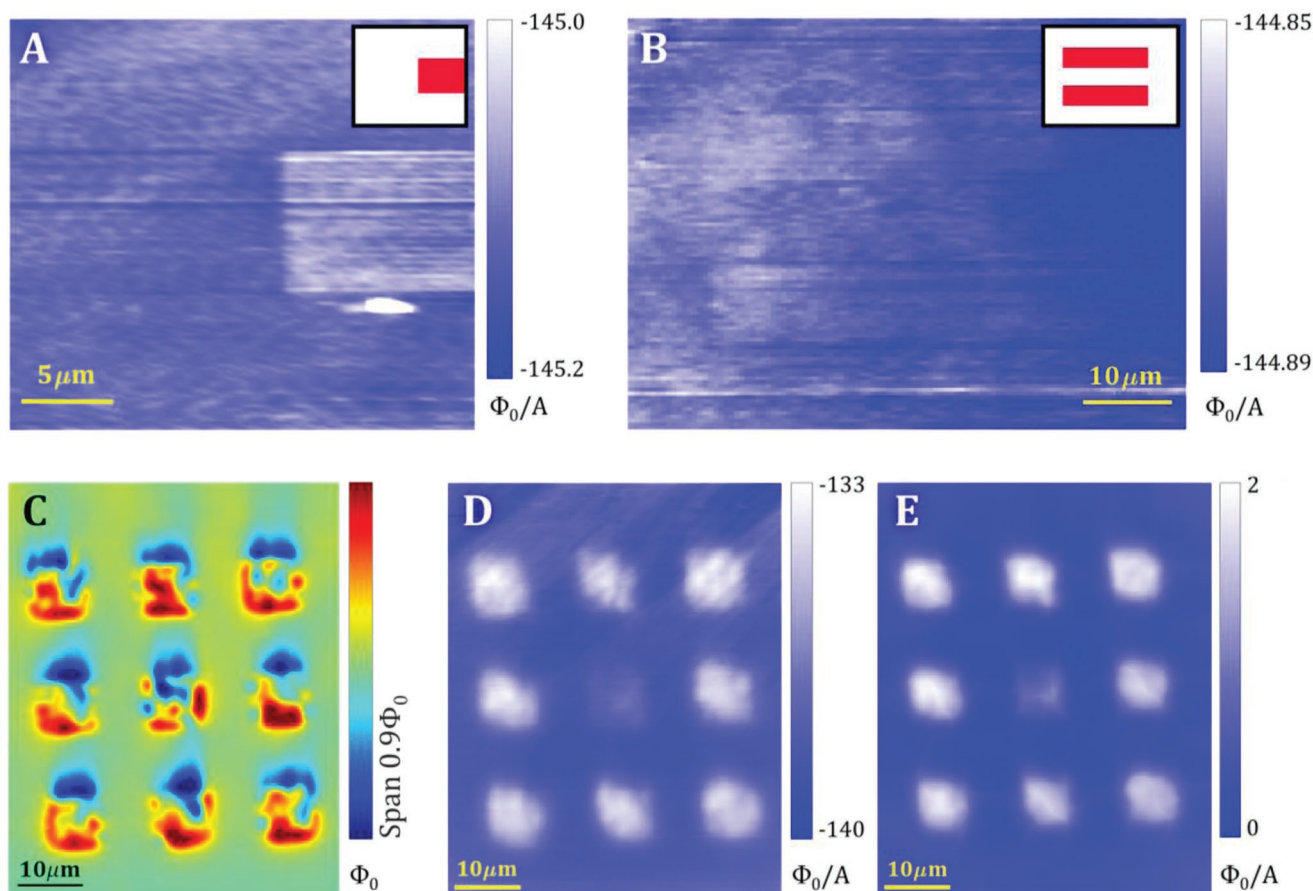


**Figure 4.** Susceptometry images of an Au(3 nm)/Nb(60 nm) bilayer film with rectangular islands of adsorbed A) ChMs and B) non-chiral molecules, taken at 4.2 K. Insets depicting the approximate location of the adsorbed areas to assist identifying the signal. C) Magnetometry image of 7 nm thick Ni islands capped by a 7 nm thick Au layer to prevent oxidation ( $10 \times 10 \mu\text{m}^2$  in area) deposited onto a 60 nm thick Nb film. D,E) Susceptometry images of the same area depicted in (C) taken below  $T_C$  (at 4.2 K) and above  $T_C$  (at 14 K), respectively.

spectroscopy.<sup>[23–27]</sup> This can be particularly appreciated with respect to the observation<sup>[25]</sup> that conductance spectra showing discrete Yu-Shiba-Rusinov states evolve to spectra consistent with chiral  $p$ -wave order parameter with increasing ChMs-adsorption density on NbSe<sub>2</sub>. Related edge-states can yield reduced superfluid density, and our data confirm the existence of such reduced superconductivity on the perimeter of the ChMs-islands. Our results are also consistent with STS measurements performed on monolayer Fe islands grown on Re,<sup>[21]</sup> and monolayer CrBr<sub>3</sub> grown on NbSe<sub>2</sub><sup>[22]</sup> ( $S$ – $F$  bilayers). In both these  $S$ – $F$  systems, the tunneling spectra were significantly altered at their perimeter compared their interior and to the bare superconductor, revealing<sup>[21]</sup> increased in-gap states density or the appearance<sup>[22]</sup> of a zero-bias conductance peak. Our data are also in accordance with the STS study of the transition metal dichalcogenide 4Hb-TaS<sub>2</sub> that consists of alternating stacks of superconducting 1H-TaS<sub>2</sub> and strongly correlated 1T-TaS<sub>2</sub>, where evidence for the existence of edge modes running along the 1H-layer terminations were found in the tunneling spectra.<sup>[52]</sup> There too, spectra measured close to the step edge show a much shallower gap compared with the 1H plane. All these STS observations are consistent with the enhanced susceptibility signal we observe only at the edges of

the ChMs islands in our SQUID measurements. As discussed above, the enhanced susceptibility can signify either reduced diamagnetism or emergent superconducting-related paramagnetic edge-states at the island perimeter, or a combination of both. Paramagnetic edge-states have been theoretically predicted to exist in some superconducting systems (e.g., quasi 1D organic superconductors),<sup>[53]</sup> but were never observed.

Previous studies of ChMs/superconductor systems demonstrated the consequent manifestation of unconventional superconductivity and the similarities between the effects of ChMs-adsorption to the effects of magnetic impurities on the surface of the superconductor. These observations suggested the possible existence of topological superconductivity in the ChMs/Nb system. Our work here, revealing susceptibility modulations situated on the edges of islands of adsorbed ChMs, agrees with the scenario of edge-states confined around the islands and provides visual support to it. The presented “designer material” of patterned hybrid ChMs on a superconductor studied here provides a promising platform for achieving patterned unconventional superconducting regions. This system may also enable to easily control and manipulate the geometry of the edges-states by selective adsorption on standard superconducting materials.

### 3. Conclusion

Reduced diamagnetism, possibly accompanied by paramagnetism, develops at the perimeter of islands of ChMs adsorbed on Nb. This apparent reduction in superconductivity is in accordance with STS measurements performed on ferromagnetic islands grown on a conventional superconductor and is attributed to topological superconductivity and edge-states. Such states are expected to exist in systems comprising a 2D magnetic monolayer adsorbed on the surface of a superconductor. Here, we show that a layer of adsorbed ChMs acts as a 2D magnetic system, while the free-standing ChMs are non-magnetic. Together with previous observations of unconventional spin-triplet superconductivity induced in a conventional superconductor upon the adsorption of ChMs, we suggest that our present results can also be associated with the emergence of topological superconductivity in these systems, although theoretical work examining this conjecture is required. Nevertheless, our present work extends the range of phenomena related to the unique effects adsorbed ChMs have on a conventional superconductor, enabling the manipulation of topological edge-states by selective adsorption, thus opening new paths for the realization of shape-controlled topological phases.

### 4. Experimental Section

**Samples Fabrication:** The Nb (60 nm) and Au(3 nm)/Nb(60 nm) thin films were grown onto a SiO<sub>2</sub>(300 nm)/Si substrate by direct current magnetron sputtering in an ultrahigh vacuum deposition chamber with a base pressure < 10<sup>-8</sup> Torr. Deposition rates of 0.35 and of 0.30 nm s<sup>-1</sup> were used for Nb and Au, respectively. The Au/Nb thin film bilayers were grown in the same chamber without breaking vacuum.

Selective adsorption of  $\alpha$ -helix L-polyalanine (L-AHPA) [[H]-CAAAAKAAAAKAAAAKAAAAKAAAAKAAAAK-[OH]] molecules (C stands for cysteine, A for alanine, and K for lysine), manufactured by Sigma-Aldrich, was obtained by defining micron-scale squares and rectangular structures into a poly(methyl methacrylate) (PMMA) resist layer, where the Nb or Au/Nb substrates were exposed, followed by chemical adsorption of the molecules onto the opened areas via an overnight soak in 1 mM solution of the molecules in ethanol in a nitrogen environment.<sup>[26,27]</sup> The remaining PMMA was then removed with acetone, followed by cleaning with isopropanol.

**Scanning SQUID Measurements:** SQUID is a non-invasive magnetic flux detector. Using a SQUID as local probe (with a small sensing loop or a small SQUID) in a scanning configuration allowed for mapping the static magnetic landscape. The probing area of the SQUID is composed of concentric pick-up loop (inner sensing loop) and excitation field coil (outer loop), as illustrated in Figure 1B.<sup>[54]</sup> Away from the probing region, the field coil and the pick-up loop are shielded using superconducting Nb films to avoid capturing signals from field sources that are not under the pick-up loop. Alternating currents (0.1–2 mA, with frequencies in the range 1–1.5 kHz) were applied to the field coil. The local susceptibility response was measured to this alternating magnetic field using the pick-up loop. The local susceptibility was measured in units of  $\Phi_0/A$ : the flux in the SQUID pick-up loop over the current in the field-coil.<sup>[35]</sup>

### Supporting Information

Supporting Information is available from the Wiley Online Library or from the author.

### Acknowledgements

M.O. and T.R.D. contributed equally to this work. This research was supported in parts by the Niedersachsen Ministry of Science and Culture and a grant from the Academia Sinica – Hebrew University Research Program (O.M. and Y.P.). O.M. thanks support from the Harry de Jur Chair in Applied Science. A.D.B. acknowledges support from a Sofja Kovalevskaja Grant endowed by the Alexander von Humboldt foundation and from the Deutsche Forschungsgemeinschaft (DFG9 Priority program SPP 2244 (grant no. 443404566)). T.R.D., E.P., A.V.B., and B.K. were supported by the European Research Council grant no. ERC-2019-COG-866236, the Israeli Science Foundation grant no. ISF-1251/19, and the Pazy Research Foundation grant no. 107-2018.

### Conflict of Interest

The authors declare no conflict of interest.

### Data Availability Statement

Research data are not shared.

### Keywords

chiral molecules, magnetic properties, SQUID, superconductivity

Received: August 28, 2022  
Revised: November 13, 2022  
Published online: February 2, 2023

- [1] M. Eschrig, *Rep. Prog. Phys.* **2015**, *78*, 104501.
- [2] J. Linder, J. W. A. Robinson, *Nat. Phys.* **2015**, *11*, 307.
- [3] F. S. Bergeret, A. F. Volkov, K. B. Efetov, *Rev. Mod. Phys.* **2005**, *77*, 1321.
- [4] M. Eschrig, T. Löfwander, *Nat. Phys.* **2008**, *4*, 138.
- [5] R. S. Keizer, S. T. B. Goennenwein, T. M. Klapwijk, G. Miao, G. Xiao, A. Gupta, *Nature* **2006**, *439*, 825.
- [6] M. S. Anwar, F. Czeschka, M. Hesselberth, M. Porcu, J. Aarts, *Phys. Rev. B* **2010**, *82*, 100501.
- [7] J. W. A. Robinson, J. D. S. Witt, M. G. Blamire, *Science* **2010**, *329*, 59.
- [8] A. Di Bernardo, S. Diesch, Y. Gu, J. Linder, G. Divitini, C. Ducati, E. Scheer, M. G. Blamire, J. W. A. Robinson, *Nat. Commun.* **2015**, *6*, 8053.
- [9] Y. Kalcheim, O. Millo, A. Di Bernardo, A. Pal, J. W. A. Robinson, *Phys. Rev. B* **2015**, *92*, 060501.
- [10] S. Diesch, P. Machon, M. Wolz, C. Sürgers, D. Beckmann, W. Belzig, E. Scheer, *Nat. Commun.* **2018**, *9*, 5248.
- [11] J. A. Ouassou, A. Pal, M. Blamire, M. Eschrig, J. Linder, *Sci. Rep.* **2017**, *7*, 1932.
- [12] S. Nadj-Perge, I. K. Drozdov, J. Li, H. Chen, S. Jeon, J. Seo, A. H. MacDonald, B. A. Bernevig, A. Yazdani, *Science* **2014**, *346*, 602.
- [13] H. Kim, A. Palacio-Morales, T. Posske, L. Rózsa, K. Palotás, L. Szunyogh, M. Thorwart, R. Wiesendanger, *Sci. Adv.* **2018**, *4*, eaar5251.
- [14] M. Ruby, F. Pientka, Y. Peng, F. von Oppen, B. W. Heinrich, K. J. Franke, *Phys. Rev. Lett.* **2015**, *115*, 197204.
- [15] R. Pawlak, M. Kisiel, J. Klinovaja, T. Meier, S. Kawai, T. Glatzel, D. Loss, E. Meyer, *npj Quantum Inf.* **2016**, *2*, 16035.
- [16] J. Li, T. Neupert, Z. Wang, A. H. MacDonald, A. Yazdani, B. A. Bernevig, *Nat. Commun.* **2016**, *7*, 12297.

- [17] J. Röntynen, T. Ojanen, *Phys. Rev. Lett.* **2015**, *114*, 236803.
- [18] S. Rachel, E. Mascot, S. Cocklin, M. Vojta, D. K. Morr, *Phys. Rev. B* **2017**, *96*, 205131.
- [19] G. C. Ménard, S. Guissart, C. Brun, R. T. Leriche, M. Trif, F. Debontridder, D. Demaille, D. Roditchev, P. Simon, T. Cren, *Nat. Commun.* **2017**, *8*, 2040.
- [20] K. Björnson, A. M. Black-Schaffer, *Phys. Rev. B* **2018**, *97*, 140504.
- [21] A. Palacio-Morales, E. Mascot, S. Cocklin, H. Kim, S. Rachel, D. K. Morr, R. Wiesendanger, *Sci. Adv.* **2019**, *5*, eaav6600.
- [22] S. Kezilebieke, M. N. Huda, V. Vaňo, M. Aapro, S. C. Ganguli, O. J. Silveira, S. Głodzik, A. S. Foster, T. Ojanen, P. Liljeroth, *Nature* **2020**, *588*, 424.
- [23] H. Alpern, E. Katzir, S. Yochelis, N. Katz, Y. Paltiel, O. Millo, *New J. Phys.* **2016**, *18*, 113048.
- [24] T. Shapira, H. Alpern, S. Yochelis, T.-K. Lee, C.-C. Kaun, Y. Paltiel, G. Koren, O. Millo, *Phys. Rev. B* **2018**, *98*, 214513.
- [25] H. Alpern, K. Yavilberg, T. Dvir, N. Sukenik, M. Klang, S. Yochelis, H. Cohen, E. Grosfeld, H. Steinberg, Y. Paltiel, O. Millo, *Nano Lett.* **2019**, *19*, 5167.
- [26] N. Sukenik, H. Alpern, E. Katzir, S. Yochelis, O. Millo, Y. Paltiel, *Adv. Mater. Technol.* **2018**, *3*, 1700300.
- [27] H. Alpern, M. Amundsen, R. Hartmann, N. Sukenik, A. Spuri, S. Yochelis, T. Prokscha, V. Gutkin, Y. Anahory, E. Scheer, J. Linder, Z. Salman, O. Millo, Y. Paltiel, A. Di Bernardo, *Phys. Rev.* **2021**, *5*, 114801.
- [28] O. Ben Dor, S. Yochelis, A. Radko, K. Vankayala, E. Capua, A. Capua, S.-H. Yang, L. T. Baczewski, S. S. P. Parkin, R. Naaman, Y. Paltiel, *Nat. Commun.* **2017**, *8*, 14567.
- [29] H. Al-Bustami, G. Kopolovitz, D. Primc, S. Yochelis, E. Capua, D. Porath, R. Naaman, Y. Paltiel, *Small* **2018**, *14*, 1801249.
- [30] R. Naaman, Y. Paltiel, D. H. Waldeck, *Nat. Rev. Chem.* **2019**, *3*, 250.
- [31] K. Pöyhönen, I. Sahlberg, A. Westström, T. Ojanen, *Nat. Commun.* **2018**, *9*, 2103.
- [32] D. Jiang, Y. Pan, S. Wang, Y. Lin, C. M. Holland, J. R. Kirtley, X. Chen, J. Zhao, L. Chen, S. Yin, Y. Wang, *Sci. Bull.* **2021**, *66*, 425.
- [33] R. Doll, M. Näbauer, *Phys. Rev. Lett.* **1961**, *7*, 51.
- [34] R. C. Jaklevic, J. Lambe, A. H. Silver, J. E. Mercereau, *Phys. Rev. Lett.* **1964**, *12*, 159.
- [35] E. Persky, I. Sochnikov, B. Kalisky, *Annu. Rev. Condens. Matter Phys.* **2022**, *13*, 385.
- [36] J. Clarke, A. I. Braginski, *The SQUID Handbook*, Vol. 1, Wiley, Hoboken, NJ **2004**.
- [37] J. R. Kirtley, *Rep. Prog. Phys.* **2010**, *73*, 126501.
- [38] N. C. Koshnick, M. E. Huber, J. A. Bert, C. W. Hicks, J. Large, H. Edwards, K. A. Moler, *Appl. Phys. Lett.* **2008**, *93*, 243101.
- [39] T. N. H. Nguyen, D. Solonenko, O. Selyshchev, P. Vogt, D. R. T. Zahn, S. Yochelis, Y. Paltiel, C. Tegenkamp, *J. Phys. Chem. C* **2019**, *123*, 612.
- [40] N. Goren, S. Yochelis, G. Jung, Y. Paltiel, *Appl. Phys. Lett.* **2021**, *118*, 172401.
- [41] P. Y. Bruice, *Organic Chemistry*, 3rd ed., Prentice-Hall, Hoboken, NJ **2001**.
- [42] N. Sukenik, F. Tassinari, S. Yochelis, O. Millo, L. T. Baczewski, Y. Paltiel, *Molecules* **2020**, *25*, 6036.
- [43] W. V. Pogosov, A. L. Rakhmanov, V. V. Moshchalkov, *Phys. Rev. B* **2003**, *67*, 014532.
- [44] D. Shvarts, M. Hazani, B. Y. Shapiro, G. Leitus, V. Sidorov, R. Naaman, *EPL* **2005**, *72*, 465.
- [45] E. Katzir, S. Yochelis, F. Zeides, N. Katz, Y. Kalcheim, O. Millo, G. Leitus, Y. Myasodeyov, B. Ya. Shapiro, R. Naaman, Y. Paltiel, *Phys. Rev. Lett.* **2012**, *108*, 107004.
- [46] I. Carmeli, G. Leitus, R. Naaman, S. Reich, Z. Vager, *J. Chem. Phys.* **2003**, *118*, 10372.
- [47] P. Crespo, R. Litrán, T. C. Rojas, M. Multigner, J. M. de la Fuente, J. C. Sánchez-López, M. A. García, A. Hernando, S. Penadés, A. Fernández, *Phys. Rev. Lett.* **2004**, *93*, 087204.
- [48] P. Dutta, S. Pal, M. S. Seehra, M. Anand, C. B. Roberts, *Appl. Phys. Lett.* **2007**, *90*, 213102.
- [49] S. Yoon, K. H. Han, B. J. Suh, Z. H. Jang, J. H. Kim, D.-Y. Jung, *J. Korean Phys. Soc.* **2012**, *60*, 1078.
- [50] I. Carmeli, V. Skakalova, R. Naaman, Z. Vager, *Angew. Chem., Int. Ed.* **2002**, *41*, 761.
- [51] R. Naaman, Z. Vager, *Phys. Chem. Chem. Phys.* **2006**, *8*, 2217.
- [52] A. K. Nayak, A. Steinbok, Y. Roet, J. Koo, G. Margalit, I. Feldman, A. Almoalem, A. Kanigel, G. A. Fiete, B. Yan, Y. Oreg, N. Avraham, H. Beidenkopf, *Nat. Phys.* **2021**, *17*, 1413.
- [53] K. Sengupta, I. Žutić, H.-J. Kwon, V. M. Yakovenko, S. D. Sarma, *Phys. Rev. B* **2001**, *63*, 144531.
- [54] M. E. Huber, N. C. Koshnick, H. Bluhm, L. J. Archuleta, T. Azua, P. G. Björnsson, B. W. Gardner, S. T. Halloran, E. A. Lucero, K. A. Moler, *Rev. Sci. Instrum.* **2008**, *79*, 053704.